J Ther Eng, Vol. 11, No. 4, pp. 991−1010, July, 2025

Journal of Thermal Engineering
Web page info: https://jten.yildiz.edu.tr
DOI: 10.14744/thermal.0000959

Research Article

Computational investigation and exergy analysis of swirling flow in vortex tube

Hitesh R. THAKARE[1,*]

[1]*Department of Mechanical Engineering, SVKM's Institute of Technology, Dhule, Maharashtra, 424 001 India*

ARTICLE INFO

Article history
Received: 12 June 2024
Accepted: 13 October 2024

Keywords:
CFD; Cold Mass Ratio; Exergy Analysis; Exergy Efficiency; Temperature Separation; VT

ABSTRACT

A vortex tube is very useful in several process industries to solve the spot cooling problem. Owing to its very small size and high pressure of working fluid, experimental analysis and determination of flow parameters of vortex tube becomes very difficult task. The present work attempts to explore and utilise the philosophy of computational fluid dynamics in an effort to overcome the limitations of experimental investigations. Simulation has been performed for turbulent, swirling, compressible flow of air at various inlet pressures using Standard k–ε turbulence model. The results of the computational model are validated against experimental results as well as computational results of previously published works through comparison of temperature separation magnitude on % basis as well as non-dimensional basis. The variation between experimental and computational results is about 8%. Thereafter, grid independence of solution is checked to circumvent the errors pertaining to grid's coarseness. Previously, many of the research works on exergy analysis of vortex tube have been conducted for constant values of cold mass ratio, whilst in the present work, performance has been checked for different cold mass ratios as well as inlet pressure values. The inlet pressure values are selected pertaining to common scenario in process industries. It is inferred from the results that the computational model is able to replicate the exergetic behaviour of vortex tube with good agreement. As hypothesized at the beginning of this research, cold mass ratio is found to be indeed an important parameter from both energy as well as exergy analysis point of view. The amount of inlet total exergy is 559 W at 200 kPa, 966 W at 300 kPa, 1352.71 W at 400 kPa, 1538.86 W at 486 kPa, 1732.29 W at 500 kPa and 2174.54 W at 600 kPa inlet pressure. Maximum cold exergy efficiency of 27.77% and hot exergy efficiency of 39.39% is observed at inlet pressure of 600 kPa. Total exergy efficiency shows minimum value for cold mass ratios in the range of 0.4 to 0.6. Cold-end exergy efficiency is observed to be more affected due to inlet pressure than hot-end exergy efficiency.

Cite this article as: Thakere HR. Computational investigation and exergy analysis of swirling flow in vortex tube. J Ther Eng 2025;11(4):991−1010.

***Corresponding author.**
*E-mail address: thakare.hitesh@gmail.com

This paper was recommended for publication in revised form by Editor-in-Chief Ahmet Selim Dalkılıç

INTRODUCTION

The science of refrigeration is directly connected with day-to-day activities of human beings. The conventional methods of refrigeration such as vapour compression systems have resulted in adverse environmental effects such as Ozone Layer Depletion, Global warming due to use of CFCs as refrigerants. Moreover, conventional refrigeration systems take some time before achieving the desired application temperature. This makes then non – useful in the applications wherein spot cooling is required instantaneously. A VT refrigeration system is a desirable mechanism in such scenarios wherein it generates hot and cold streams of air instantaneously from input stream of pressurized fluid admitted through the tangentially placed inlet. The fluid from a cold stream and hot stream are taken out at reverse ends through the cold end and hot end respectively. It was designed by Ranque [1] and studied by Hilsch [2]. A VT uses natural refrigerants such as air and creates a refrigeration effect in the absence of any chemical reaction. Also, the structure and construction of VT is very simple and robust. It involves no moving parts except the hot-end control valve. This leads to maintenance-free operation of VT for a prolonged period. Besides, its small size required to create a substantial temperature difference makes it a favourite candidate for applications involving space constraints such as cooling suits of foundry workers, cold air circulation in blow moulded fuel tanks, spot cooling in soldering of toothpaste tubes, ultrasonic weld cooling, gas liquefaction [3,4], cooling of welded components to improve productivity & profits in fabrication process [5] to name a few. Users can also obtain precise control over the temperatures obtained from VT through the proper operation of the conical control valve situated at the hot end.

The performance of VT is assessed using the following parameters

a. Temperature change at the cold end given as change in temperature of inlet air and air exiting through the cold end. Mathematically,

$$\Delta T_c = T_i - T_c \tag{1}$$

b. Temperature change at the hot end given as change in temperature of inlet air and air exiting through the hot end. Mathematically,

$$\Delta T_h = T_h - T_i \tag{2}$$

c. Cold mass ratio – the ratio of cold fluid mass exiting through of cold side to the entering fluid mass at the inlet. Mathematically,

$$\mu_c = \frac{m_c}{m_i} \tag{3}$$

Literature Review

Due to its striking constructional and operational features, VT continued to be the topic of several scientific studies ever since it was discovered by Ranque [1] in 1931. Wu et al. [3] modified the design for VT nozzle and observed that improved nozzle design created lower temperature by 5°C compared to Archimedes' spiral nozzle and 2.2°C lower than normal rectangular nozzle. Kirmaci [4] reported that temperature variation magnitude reduced when inlet number of nozzles increased. Experimental investigation done by Saidi and Yazdi [6] along with exergy model analysis indicated that the magnitude of exergy destruction reduced when inlet pressure was increased. Aljuwayhel et al. [7] reported that reduction in diameter from 3 cm to 1.5 helped to improve cold side temperature drop by 4.4%. The work of Tarasova et al. [8] focused on low pressure VTs & observed that the exergy efficiency of the dust-trapping process was very small thereby making the process ineffective. Kirmaci et al. [9] reported that Argon exhibited a higher magnitude of temperature separation than air and oxygen. The inlet exergy was observed to rise exponentially with rise in pressure at inlet. Dincer et al. [10] reported that the cascading arrangement's exergy efficiency was higher than that for classical VT.

Dutta et al. [11] performed a computational study on VT & reported a significant amount of backflow of atmospheric air into VT at higher values of hot mass ratio which results in higher temperature at cold end. Baghdad et al. [12] carried out CFD analysis and exergy study of using CO_2. Results indicated that at all inlet pressure values, total exergy losses were highest for cold mass ratio of 0.1 and 0.9 and minimum values were seen for cold mass ratio of 0.4 and 0.6. Khazaei et al. [13] reported that the predictions of Standard $k - \varepsilon$ model were improved than other turbulence models in most of the regions. Bej and Sinhamahapatra [14] carried out CFD modelling of the cascading arrangement of VT at hot end using the Standard $k - \varepsilon$ model and reported hot exergy reduction with the rise in cold ratio. Manimaran [15] reported that the trapezoidal inlet of VT provided better temperature separation than the rectangular design. Moraveji and Toghraie [16] reported a reduction in the temperature of hot as well as cold exit with an increase in number of inlets. Devade and Pise [17] reported that with higher cold-end diameter, exergy losses were reduced. With an increase in inlet pressure, exergy loss was observed to increase. Kirmaci et al. [18] carried out an experimental and exergy study of VT using different materials and working fluids at various inlet pressures. Loss of exergy was observed to be more for steel as nozzle material than fibreglass and aluminium due to higher thermal resistance value of steel. Jain et al. [19] reported that the exergy analysis of the transcritical cycle revealed that usage of VT in place of expansion reduced exergy losses. Kaya et al. [20] reported that with an increase in the number of orifices in the inlet nozzle, specific outlet exergy was observed to increase.

Aghagoli and Sorin [21] reported that with an increase in entry pressure, maximum value of exergy efficiency was obtained at a lesser cold mass ratio. Lagrandeur et al. [22] observed that with a rise in inlet pressure, a higher % of inlet mechanical exergy transformed into thermal exergy. Wang

and Suen [23] observed higher cooling and heating effect produced by air than other refrigerants due to higher magnitude of tangential shear stress in radial direction for air. He et al. [24] stated that the highest temperature change was noted for air while it was minimum for carbon tetrafluoride. The temperature separation was affected by all gas properties. Jain et al. [25] reported that exergetic efficiency of transcritical cycle with VT was about 9.17% to 11.68% higher than that of cycle using expansion valve. Liang et al. [26] studied the result of the shape of vortex generator made of various materials and reported the resin vortex generator to provide highest energy separation and exergy efficiency due to lower thermal conductivity of resin. Shahsavar et al. [27] studied the application of VT to replace water bath in photovoltaic system and reported that exergy efficiency was about 19.46% and this system helped to save 27.7 tons of CO_2 per year. Qatarani nejad et al. [28] considered the use of VT in a gas station to avoid usage of natural gas in water bath heaters. This project helped to save 8.55 tons of CO_2 per year by producing 42770.58 kW.

Experimental study of Yadav et al. [29] used modified VT having dual flow, one solid plug near cold end #1 and one hollow plug near cold end #2. Optimum performance was obtained for hollow and solid cone angles of 45° and 55° respectively. Devade and Pise [30] studied the effect of several geometrical and operational parameters such as L/D ratio, number of nozzles, valve angles, tube geometry and inlet pressure. Authors also proposed a non-dimensional correlation for temperature separation. Authors reported maximum COP at L/D ratio of 17 which decreases with increase in L/D ratio. Noor et al. [31] carried out CFD analysis and observed higher COP for parallel flow VT than counter flow VT. Bagre et al. [32] computationally studied elliptical vortex tube and reported an improvement of 49.89% in energy separation.

Gap identified from published literature and importance of exergy analysis of a thermal system

Generally, analysis of VT is done in terms of the magnitude of cold and hot side temperature change at various cold mass ratio values. Thus, most of the works are based on energy and mass balance analysis of VT. However, as it is well known that energy analysis expresses only the quantity of energy as per the First Law of Thermodynamics and it does not convey the essential information about quality of energy as well as its degradation occurring during a process by the virtue of irreversibility. On the contrary, exergy analysis takes into account both the 1st and 2nd Law of Thermodynamics. In essence, exergy investigation of a thermal system is highly essential since it is an indicator of quality of energy. Furthermore, it is vital to note that most of the works concerning the exergy analysis of VT [4,9,17,18,20] have been performed at a constant value of μ_c. Very few works [6,10,14] have been carried out for range of μ_c values which is an important performance indicator of VT. It is essential to investigate the exergetic performance of VT at different inlet pressure values as well as cold mass ratios, simultaneously. To our best understanding of published literature, such an investigation was seldom reported. Besides, it has been observed that there are several areas in a process industry wherein different working pressures of air are readily available as a process requirement. However, a precise understanding of its utilization from exergy point of view needs to be elaborated. Hence, studying the behaviour of VT at various magnitudes of inlet pressures becomes imperative. The VT's performance is significantly affected by multiple constructional and operational parameters, which has led to incongruity about its flow physics and performance prediction among the researchers, despite of numerous investigations of various types and methodologies carried out. Owing to its small dimensions, the precise determination of various parameters of flow physics of VT is a complex task during the experimentation. For example, during the study of Ahlborn and Groves [33], a 1.6 mm diameter pitot tube used as a probe in VT of 25.4 mm diameter blocked about 8% of the effective VT area. Most of the exergy analysis studies have been performed through experimentation, thereby limiting the extent of exploration of underlying flow physics.

In case of such ambiguity, CFD tools can be very well used to obtain insights about influential flow physics parameters which contribute towards the exergy efficiency of VT. It is well understood that numerical analysis cannot function as a substitute for experimentation. However, it can be very effective in supporting experimentation, if done systematically and diligently. Furthermore, cost and time requirements involved with CFD analysis are significantly lower than those for experimentation when CFD model is properly constructed and *validated* with experimental results. Thereafter, parametric analysis becomes possible. Previously, Aljuwayhel et al. [7], Skye et al. [34] have carried out experimental and computational analysis using commercial VT by developing 2D axisymmetric CFD model of about 25000 cells. Authors reported that their models indicated a notable difference between experimental and numerical results. Farouk and Farouk [35] used two-dimensional axisymmetric domain of VT to report important flow physics parameters such as tangential velocity, axial velocity and static temperature variation. Computational analysis performed by Shamsoddini et al. [36] used an axisymmetric model of VT to replicate the flow physics even with multiple inlets of VT.

Objectives of the present study

The present study intends to analyse the combined effect of entry pressure and cold mass ratio on temperature separation magnitude generated in VT. Thereafter, effect of supplied pressure on exergy efficiency of VT has been studied. This paper attempts to depict the utilization of different working pressures based on exergy analysis. This will help the readers to select the inlet pressure having optimum exergy throughput during operation of VT in practical cooling applications.

Simulations are performed up to inlet pressure value of 600 kPa to examine the effect of the increase in pressure on the exergy efficiency of VT. The CFD results are equated with experimental ones firstly to validate them. Thereafter, the influence of cold mass ratio on temperature change performance and exergy efficiency has been investigated. Thus, the definitive purposes of this study are

1. To create a reliable computational model of VT and validate its output by comparing the results with experimental results.
2. To observe the change of exergy efficiency with cold mass ratio and entry pressures.

This manuscript consists of 3 sections. Section 1 elaborates fundamental characteristics of VT along with its pertinent applications and a detailed review of previously published literature. Section 2 describes in details the methodology of CFD analysis as well as the underlying mathematics involved in exergy analysis of VT. Section 3 presents a discussion about results obtained from CFD analysis for exergy study of VT.

DATA REDUCTION FOR CFD INVESTIGATION OF VT

Modelling of Physics using Mathematical Equations

Conservation equations

The conservation equations have been solved using Ansys Fluent™ 2022. These are equations for conservation of energy, momentum and mass accompanied by equation of state. These equations are given as

$$\frac{\partial \rho}{\partial t} + \nabla.\left(\rho \vec{v}\right) = S_m \tag{4}$$

$$\frac{\partial}{\partial t}\left(\rho \vec{v}\right) + \nabla.\left(\rho \vec{v}\vec{v}\right) = -\nabla p + \nabla.\left(\bar{\bar{\tau}}\right) + \rho \vec{g} + \vec{F}, \tag{5}$$

$$\frac{\partial \rho h_o}{\partial t} - \frac{\partial P}{\partial t} + \mathrm{div}(\rho h_o \mathrm{U}) = \mathrm{div}\left(\lambda \,\mathrm{grad}\, T_s\right) \tag{6}$$

$$P = \rho R T_s \tag{7}$$

Thereafter, equations are also solved for transport quantities to replicate the turbulence inside VT using Standard k – ε model, which is capable of rendering the flow field with high accuracy [34,37].

Transport equations – Standard k – ε model

There are two equations in Standard k – ε model. One for turbulence kinetic energy, k, and second one is for its rate of dissipation, ε, given as follows [38]:

$$\frac{\partial}{\partial t}\left(\rho k\right) + \frac{\partial}{\partial x_i}\left(\rho k u_i\right) = \frac{\partial}{\partial x_j}\left[\left(\mu + \frac{\mu_t}{\sigma_k}\right)\frac{\partial k}{\partial x_j}\right] + G_k + G_b - \rho\varepsilon - Y_M + S_k \tag{8}$$

$$\frac{\partial}{\partial t}\left(\rho \varepsilon\right) + \frac{\partial}{\partial x_i}\left(\rho \varepsilon u_i\right) = \frac{\partial}{\partial x_j}\left[\left(\mu + \frac{\mu_t}{\sigma_\varepsilon}\right)\frac{\partial \varepsilon}{\partial x_j}\right] + C_{1\varepsilon}\frac{\varepsilon}{k}\left(G_k + C_{3\varepsilon}G_b\right) - C_{2\varepsilon}\rho\frac{\varepsilon^2}{k} + S_\varepsilon \tag{9}$$

Equations for exergy analysis of VT

The following are the assumptions made during the exergy analysis of VT system:

1. Friction inside the VT system is negligible.
2. VT system is working at a steady state.
3. The flow in the VT system is adiabatic in nature i.e., VT is insulated and no heat exchange happens with the surroundings.
4. No chemical reaction takes places inside VT system. Thus, chemical exergy is not needed to be calculated.

Physical exergy is calculated as

$$\dot{E}_{Ph} = \dot{m}\left[C_p\left(T - T_0\right) - T_0\left(C_p \ln\left(\frac{T}{T_0}\right) - R\ln\left(\frac{P}{P_0}\right)\right)\right] \tag{10}$$

Where, $\dot{E}_{ph}$ represents physical exergy of VT system, $\dot{m}$ indicates flow rate of mass, C_p is specific heat of working fluid, T is the instantaneous temperature of fluid stream, T_0 is initial reference environment temperature 293.15 K, R is specific gas constant which is different for individual fluid, P is the instantaneous pressure of fluid stream & P_0 is reference environmental pressure of 101.325 kPa.

Kinetic exergy is calculated as

$$\dot{E}_{KN} = \dot{m}\frac{v^2}{2} \tag{11}$$

Potential exergy is calculated as

$$\dot{E}_{PT} = \dot{m}gz \tag{12}$$

The total exergy at the inlet is calculated as

$$\sum \dot{E}_i = \dot{E}_{i,PH} + \dot{E}_{i,KN} \tag{13}$$

Total exergy at hot end is calculated as

$$\sum E_h = E_{h,Ph} + E_{h,KN} + E_{h,PT} \tag{14}$$

Total exergy at cold end is calculated as

$$\sum E_c = E_{c,Ph} + E_{c,KN} \tag{15}$$

Total exergy at outlet is calculated as

$$\sum \dot{E}_o = \sum \dot{E}_{o,hot} + \sum \dot{E}_{o,cold} \tag{16}$$

The magnitude of total lost exergy is calculated as

$$\sum \dot{E}_{lost} = \sum \dot{E}_i - \sum \dot{E}_o \Rightarrow \sum E_{lost} = \sum E_i - \left(\sum E_h + \sum E_C\right) \tag{17}$$

It is recognized that II[nd] law efficiency is calculated as,

$$\eta_{II} = \frac{\text{minimum exergy required for a function}}{\text{actual exergy required for same function}} \quad (18)$$

Then, we can calculate exergy efficiency at cold end as

$$\eta_{II,cold} = \frac{\sum \dot{E}_{o,cold}}{\sum \dot{E}_i} \quad (19)$$

Also, hot-end exergy efficiency is calculated as

$$\eta_{II,hot} = \frac{\sum \dot{E}_{o,hot}}{\sum \dot{E}_i} \quad (20)$$

Thus, second law efficiency indicates how good the operation of an actual device is taking placed as compared to theoretically possible when operating conditions at the inlet and outlet are the same.

Boundary Conditions

This section describes the boundary conditions applied in current numerical study fully to maintain clarity and authenticity. The essential proportions of VT used in present analysis are shown in Figure 1. The working diameter of VT is 11.4 mm, working length in which the temperature separation process occurs is 106 mm and the diameter of the cold end is 6.2 mm. This VT is charged with different

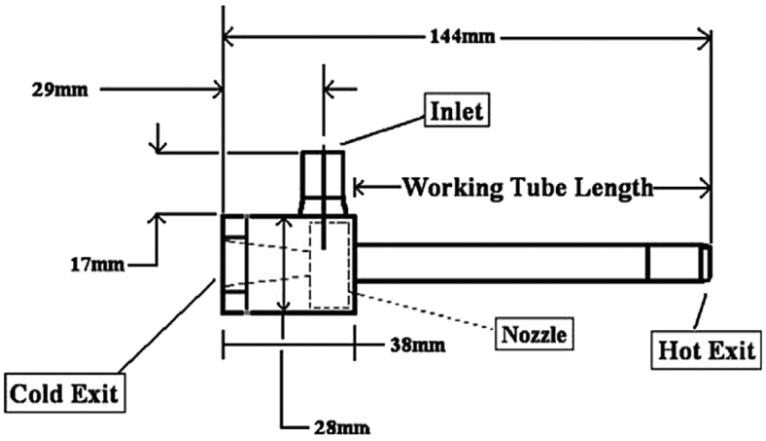

Figure 1. Essential proportions of VT used in the present study.

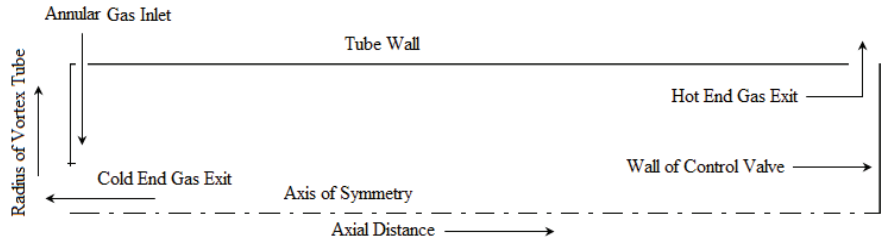

(a)

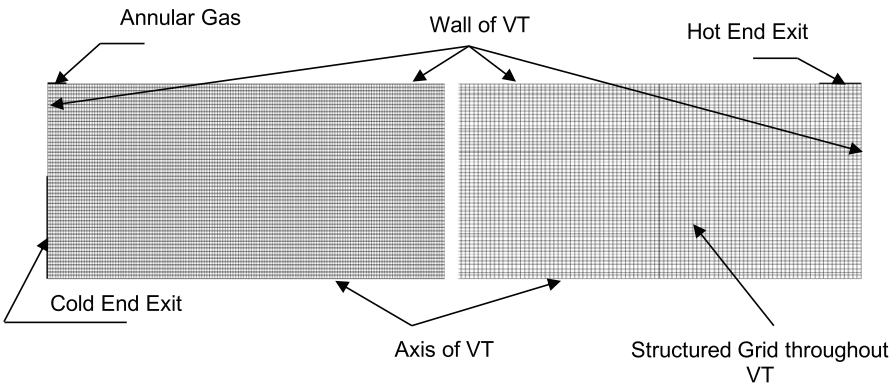

(b)

Figure 2. (a) Schematic of VT computational domain (b) Structured mesh used during CFD analysis.

working pressures. In the original experimental study, the working fluid i.e., pressurized air was admitted through six inlet nozzles. However, in the present CFD analysis, inlet is considered as annular inlet through the process described in Skye et al. [34] and Farouk and Farouk [35]. These details are not repeated here to maintain brevity. The resultant numerical domain is represented in Figure 2 (a). The computational model was generated and structured mesh was created using Ansys™ Workbench 2022 R1 as shown in Figure 2 (b).

The inlet of VT is modelled as a *mass flow inlet* for which mass flow rate, inlet total temperature, radial velocity

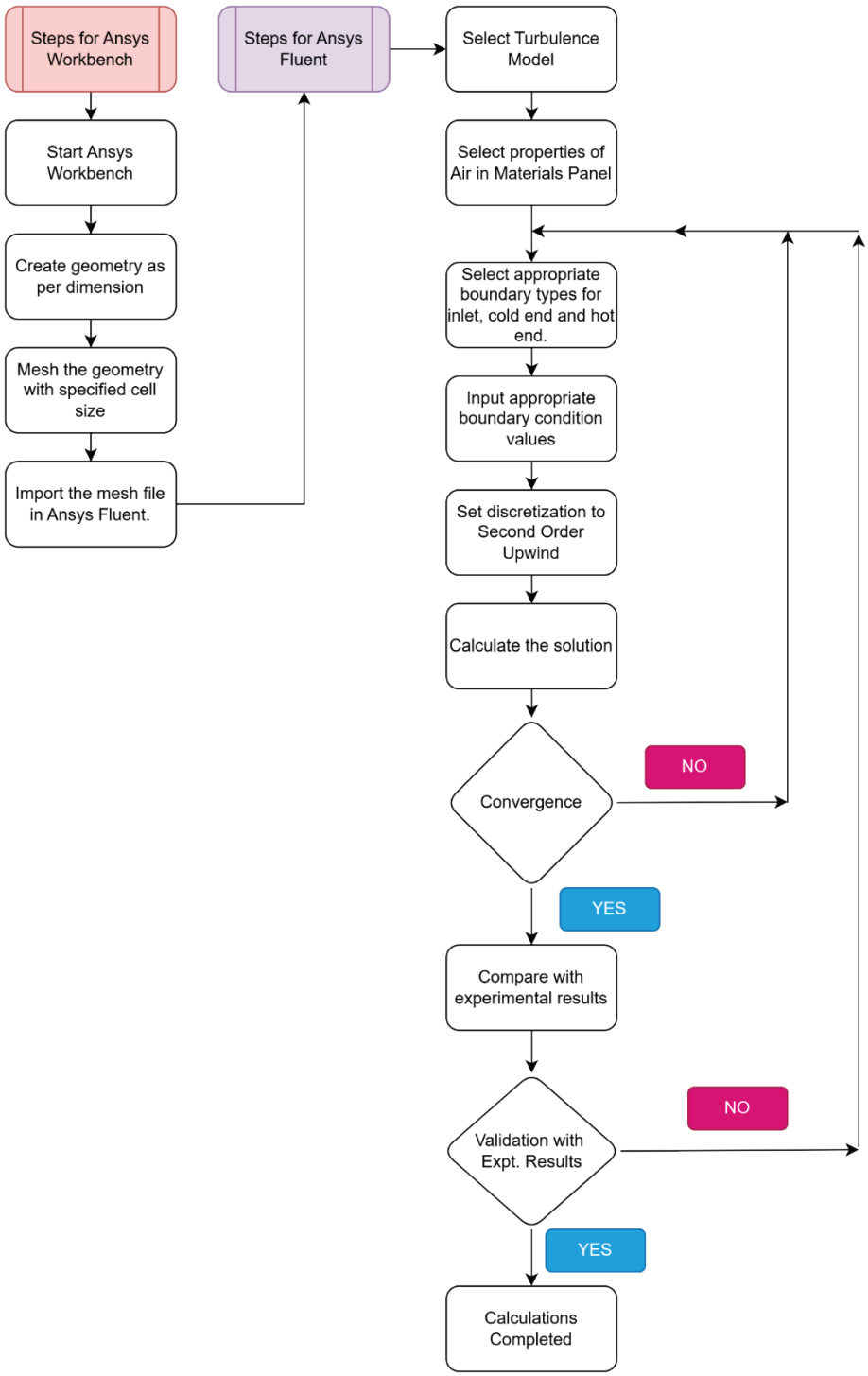

Figure 3. Flowchart of CFD simulations performed in the present study.

and tangential velocity components have been provided as input parameters. Cold outlet and hot outlet both are modelled as pressure outlets directly exposed to atmosphere. The pressure at cold outlet is atmospheric. Pressure at hot outlet is varied to get the particular value of cold mass ratio from cold end [34]. For all the simulations, energy equation is assisted with the activation of dissipative terms.

The flow inside VT is turbulent and swirling in nature & it consists of steep pressure gradients which are modelled using PRESTO! (PRessure STaggering Option) scheme. This scheme uses the discrete continuity balance for a staggered control volume about the face to compute the staggered (i.e., face) pressure. This procedure is similar in spirit to the staggered-grid schemes used with structured meshes [11,37]. The coupling of Pressure–velocity terms is attained using the SIMPLE algorithm. The values of Under Relaxation Factors have been kept as default. Convergence of solution is considered when residuals for energy are of the order of 10^{-6} and 10^{-3} for all other quantities.

The computational domain used in the present CFD study is 2D axisymmetric model which incorporates the *swirl* feature. Such a model is advantageous as it helps to use less computational power; while conserving the vital 3D features of the flow field [35]. The modelling of physics of axisymmetric flows with *swirl* has been described very well in [38]. This procedure has also been presented in Figure 3 with necessary details.

Grid Independence Study

Before proceeding for validation, the structured grid generated was examined to avoid errors arising due to the coarseness of grid as well as wastage of computational power due to an over-refined grid. This was assured by testing structured grids of diverse sizes i.e., with 14,500, 25,346, 57,000 and 1,01,308 cells. The cold side temperature for cold mass ratio of value μ_c = 0.2 has been plotted in Figure 4 for various grids. It indicates that for grid size of 25,346 and 57,000 cells, there is no noticeable change in cold end temperature. Increasing the grid size beyond 57,000 cells does not create significant changes in the results, neither it is small such as that with 25,346 cells. Hence, this grid size is chosen for further computations.

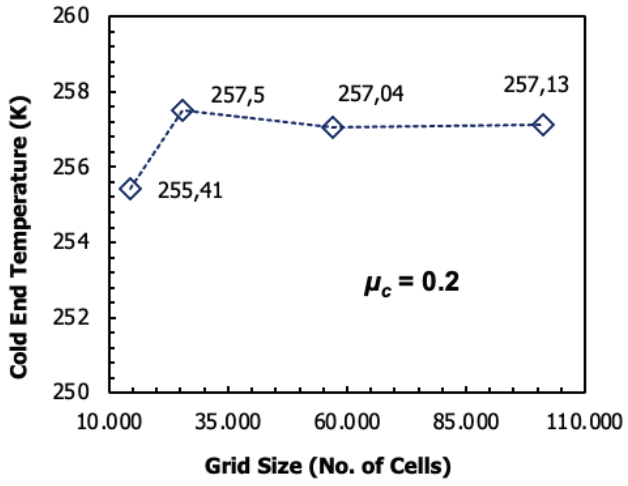

Figure 4. Grid independence study – variation of cold end temperature for different grids at μc = 0.2.

Validation

Before proceeding towards parametric analysis, it is vital to establish the authenticity of the present CFD model. For this purpose, CFD results are compared with experimental results as well as previously published computational results. Figure 5 shows temperature variation magnitude at cold exit and hot exit of VT obtained during present computational study. These are compared with the temperature separation magnitude reported in the works of Skye et al. [34], Farouk and Farouk [35] and Pourmahmoud and Akhesmeh [39] to validate and authenticate. It indicates that present CFD results are concurrent with experimental as well as previous CFD outcomes. It infers that the simulation procedure adopted in the current work is correct even though we have used the Standard k – ε model, different from Farouk and Farouk [35].

Figure 6 shows dissemination of total temperature inside VT. These contours clearly indicate the temperature separation phenomenon wherein the axial flow is at a colder temperature than inlet and directed towards cold end. Consequently, flow near the tube periphery is at greater temperature than inlet and directed towards hot end.

The accuracy of CFD results can also be compared with the help of % variation in the computation of minimum *total* temperature at cold as,

$$\%(\Delta T_c)=\frac{(\Delta T_c)_{\exp}-(\Delta T_c)_{cfd}}{(\Delta T_c)_{\exp}}\times 100 \qquad (21)$$

This % variation has been reported in Table 1 as witnessed in different studies. It indicates a reduction in % variation during the current analysis. Hereafter, this model has been utilized to carry out parametric analysis. Figure 7 depicts the variation of temperature separation magnitude and % deviation observed in various studies i.e. data from Table 1 in graphical form for ease of understanding of the readers.

Table 2 presents mass and energy balance obtained during CFD simulation for an inlet pressure of 468 kPa. This is essential to verify that the simulation procedure followed is adequate. The mass balance of the order of 10^{-6} and energy balance with less than 1% error is observed in this table. Thus, the simulation procedure of the current CFD study is adequate.

Stephan et al. [40] has provided a non-dimensional relationship about temperature separation magnitude as follows:

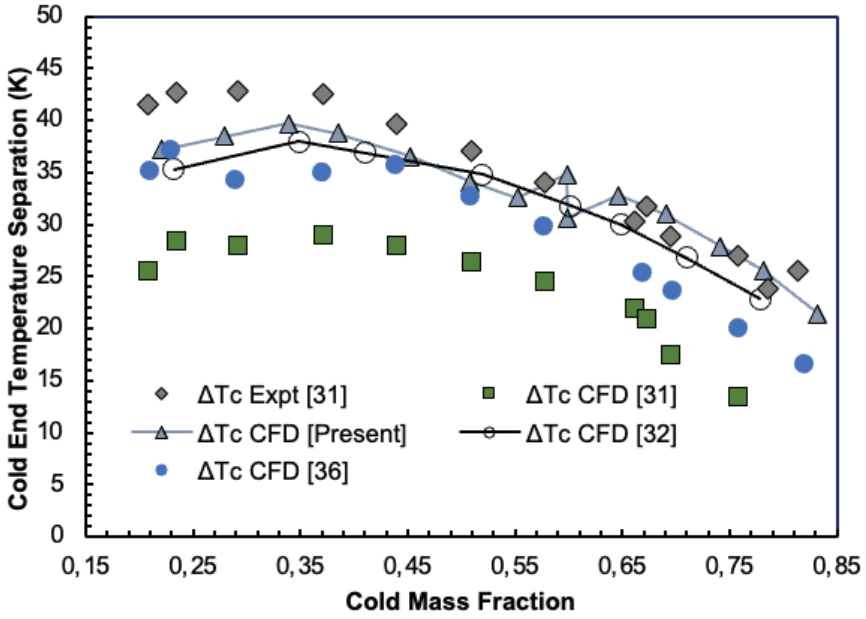

(a)

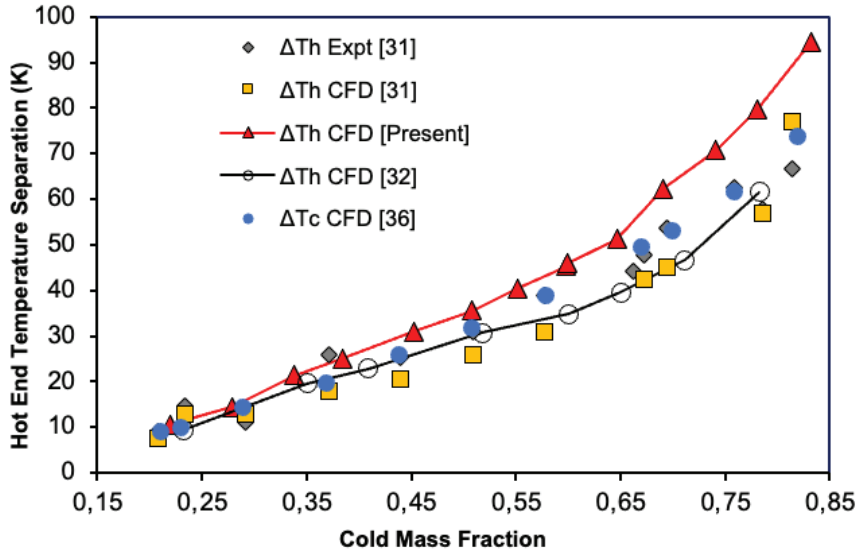

(b)

Figure 5. Validation of CFD values against experimental values (a) Cold exit temperature change magnitude (b) Hot exit temperature change magnitude.

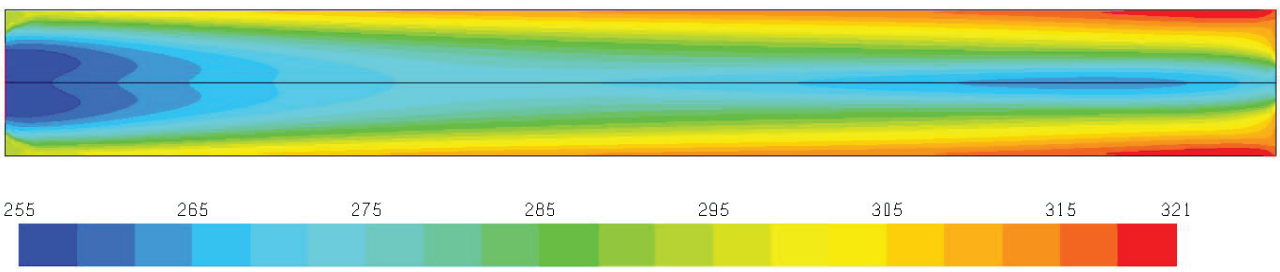

Figure 6. Contours of Total Temperature inside VT (K).

Table 1. % Deviation of minimum cold exit temperature obtained in different studies

Sr. No.	CFD Study and turbulence model used	Min. (T_c)exp	Max. $(\Delta T_c)_{exp}$= T_{in} – Min. $(T_c)_{exp}$	Min. $(T_c)_{cfd}$	Max. (ΔT_c) = T_{in} – Min. $(T_c)_{cfd}$	%(ΔT_c)
1.	Skye *et al.*, Standard k-ε [34]	251.3 K	42.9 K	265.2 K	29 K	32.40 %
2.	Farouk and Farouk, LES [35]	251.3 K	42.9 K	256.2 K	38 K	11.42 %
3.	Pourmahmoud and Akhesmeh, Standard k – ε [39]	251.3 K	42.9 K	256.9 K	37.3 K	13.11 %
4.	Standard *k* – ε [Present]	251.3 K	42.9 K	254.5 K	39.7 K	7.435 %

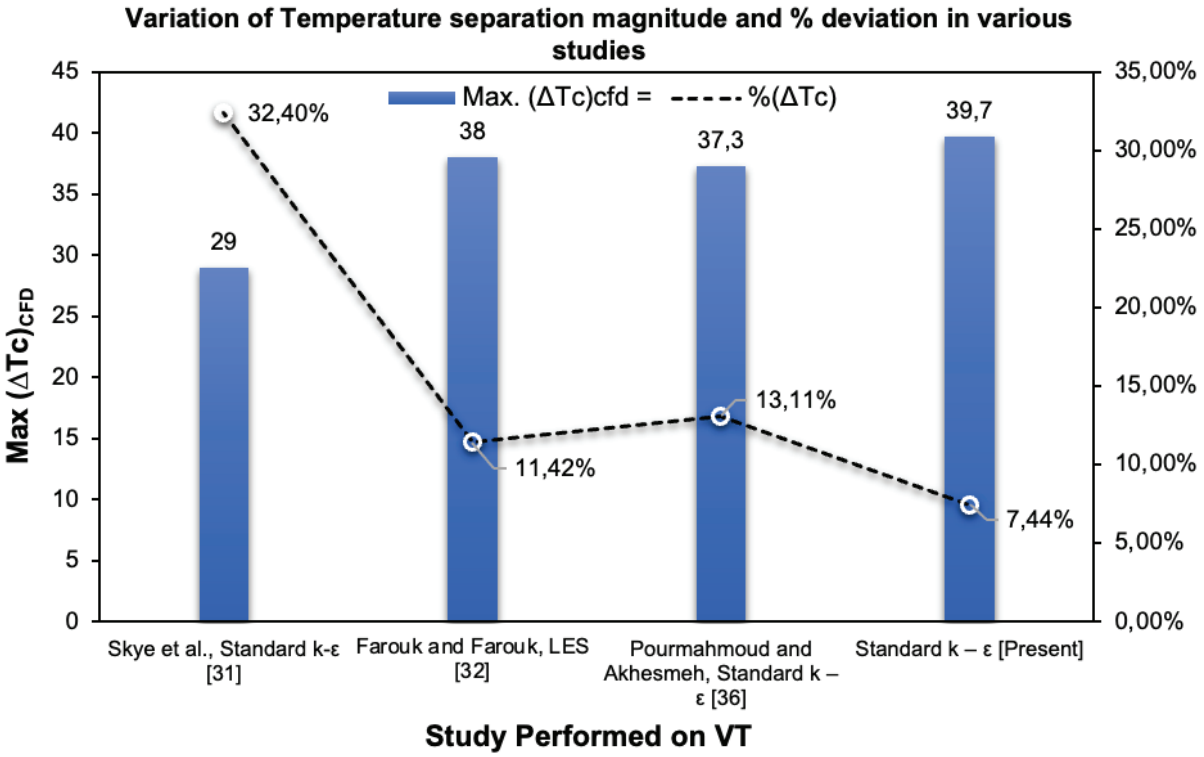

Figure 7. Variation of temperature separation magnitude and % deviation in various studies.

Table 2. Mass and energy balance obtained during CFD simulation for inlet pressure of 468 kPa

min (kg/s)	mc (kg/s)	mh (kg/s)	Mass balance	ΔE = Ein - (Ec + Eh)	%ΔE = ΔE/Ein
0.00835	0.001837	0.00653	-1.71E-05	-0.006	0.251
0.00835	0.002330	0.006016	4.20E-06	0.004	0.161
0.00835	0.002827	0.005511	1.23E-05	-0.002	0.074
0.00835	0.003210	0.005126	1.35E-05	0.000	0.003
0.00835	0.003778	0.004563	8.99E-06	-0.001	0.030
0.00835	0.004244	0.004097	9.31E-06	0.002	0.064
0.00835	0.004608	0.003734	8.18E-06	0.002	0.066
0.00835	0.004999	0.003345	6.12E-06	0.002	0.065
0.00835	0.005765	0.002578	6.55E-06	0.020	0.806
0.00835	0.006186	0.00216	4.60E-06	0.021	0.857
0.00835	0.006944	0.001403	2.45E-06	0.017	0.697

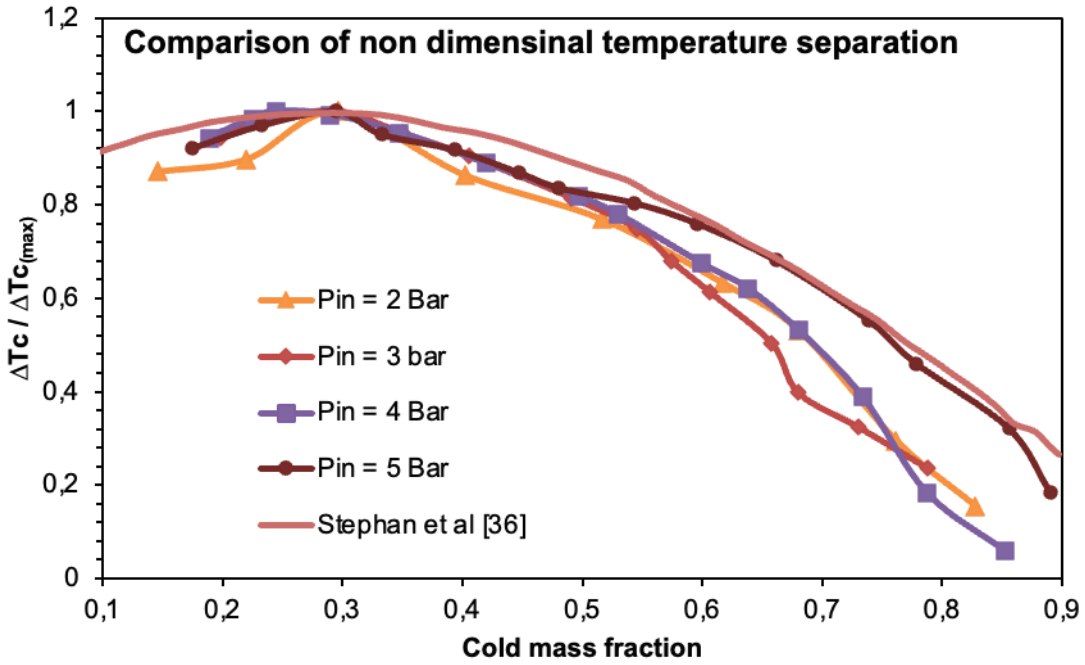

Figure 8. Comparison of present CFD results with non-dimensional correlation of Stephan et al. [40] (made by author).

$$\frac{\Delta T_c}{(\Delta T_c)_{\max}} = f(\mu_c) \tag{22}$$

It is imperative to note that this correlation is independent of operating and geometric characteristics of a VT and depends only on the value of the cold mass ratio. Hence, it can be well utilized to compare the temperature separation magnitude of various cases. Figure 8 presents a comparison of present CFD results with this non-dimensional correlation. It indicates that for all the inlet pressure values, the temperature separation magnitude is in agreement with that of Stephan et al. [40].

Once the reliability of CFD model had been validated, investigations were conducted using this computational model and methodology to study the result of entry pressure and cold mass ratio on VT's performance through exergy analysis. These results have been discussed in subsequent Section 3.

RESULTS AND DISCUSSION

It is essential to mention here that most of the works concerning the exergy analysis of VT [4, 10, 18, 19, 21] have been conducted at constant cold mass ratio. Very few works [6, 11, 15] have been carried out for a range of cold mass ratio values which is an important performance factor of VT. Hence, these works have been used as qualitative reference, wherever found appropriate. It is to be noted that operating conditions between the present work and those used in the work of Dincer et al. [10] are different, ass highlighted in Table 3. However, the work of Dincer et al. [10] has been referred to here for *qualitative comparison* due to its elaborated results, wherever appropriate.

Figure 9 shows the Comparison of hot end temperature separation magnitude (ΔTh) obtained in the present CFD work and Dincer et al. [10]. Due to different operating conditions, the magnitude of ΔTh is different. However, in both cases, this magnitude is higher for larger value of cold mass

Table 3. Operating conditions used in the present work and those in Dincer et al. [10]

Sr. No.	Operating parameter	Dincer *et al.* [10]	Present work
1.	Inlet pressure	730 kPa	600 kPa, 500 kPa, 468 kPa, 400 kPa, 300 kPa, 200 kPa,
2.	Length of VT	135 mm	106 mm
3.	Working diameter of VT	9 mm	11.4 mm
4.	Cold end diameter of VT	--	6.2 mm
5.	Number of inlet nozzles	4	6
6.	Type of exergy analysis	Hot end only	Both hot end and cold end

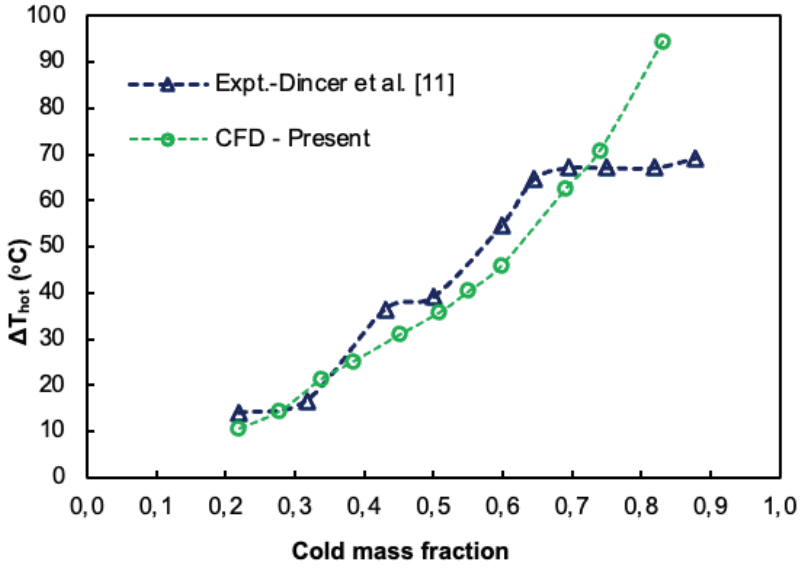

Figure 9. Correlation between of hot end temperature separation magnitude attained in current CFD work and Dincer et al. [10] (made by author).

ratio. The trend shows a good qualitative agreement. Cold exit temperature change magnitude is not available in the work of Dincer et al. [10], hence couldn't be presented here.

Figure 10 shows the variation of inlet exergy for different pressures at the inlet to VT and cold mass ratio. It is witnessed that inlet exergy rises with a rise in entry pressure but remains the same for different values of cold mass ratio. The amount of inlet total exergy is 559 W at 200 kPa, 966 W at 300 kPa, 1352.71 W at 400 kPa, 1538.86 W at 486 kPa, 1732.29 W at 500 kPa and 2174.54 W at 600 kPa inlet pressure. The highest magnitude of inlet exergy was reported at 600 kPa inlet pressure and it was lowest for inlet pressure of 200 kPa. The trend of inlet exergy of VT agrees well qualitatively with Dincer et al. [10]. The inlet exergy in this reference work was observed to be 3780.49 W at 730 kPa inlet pressure.

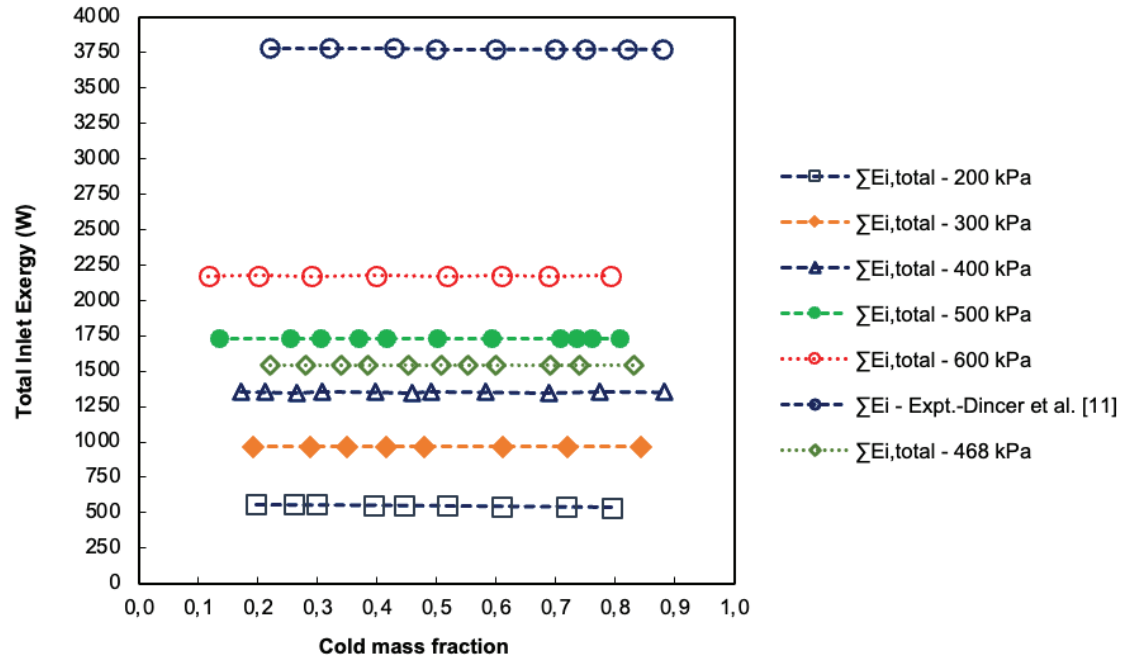

Figure 10. Total inlet exergy for different values of cold mass ratio and entry pressure.

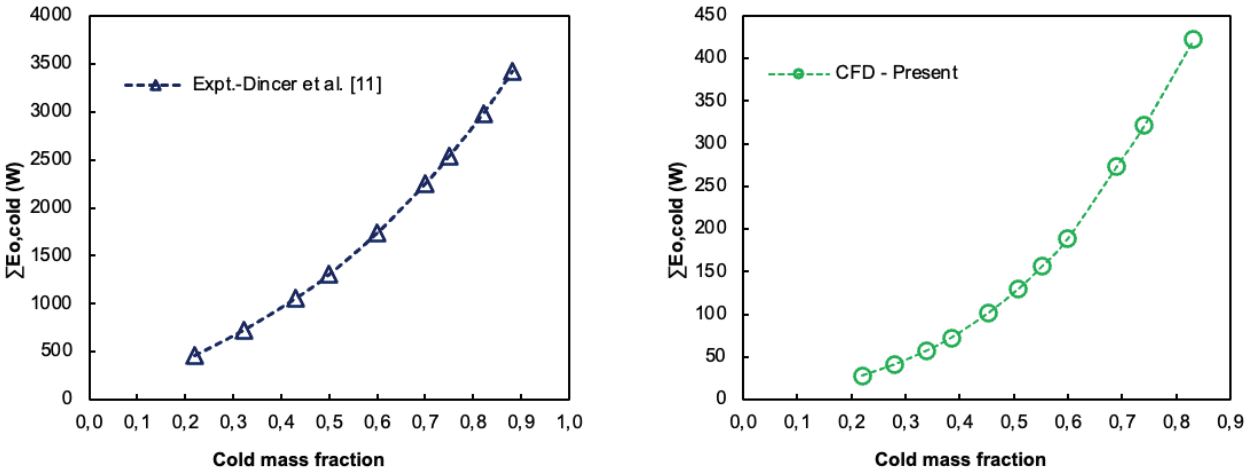

(a) (b)

Figure 11. (a) Total cold outlet exergy for different cold mass ratios for Dincer et al. [10] (b) Total cold outlet exergy for different cold mass ratios for present CFD analysis.

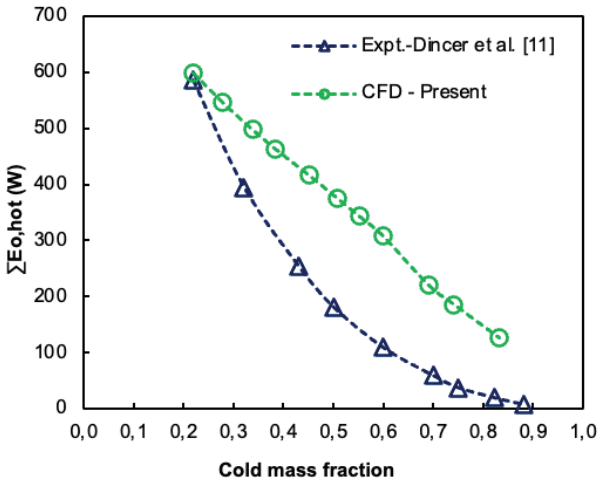

Figure 12. Total exergy at hot outlet for different values of cold mass ratio.

Figure 11 (a) and (b) shows total exit exergy variation at cold exit for different cold mass ratios at an entry pressure of 468 kPa. With rise in cold mass ratio, the cold outlet exergy magnitude goes on increasing. As expected, this magnitude is lesser in the present work than that of Dincer et al. [10] due to the lower operating pressure used in the present work. However, the general trend agrees well.

Figure 12 shows the total hot outlet exergy variation for different cold mass ratios at an entry pressure of 468 kPa. With a rise in cold mass ratio, exergy magnitude at hot exit is observed to be reducing. This can be attributed to reduced mass exiting through hot end. This ultimately results in reduced kinetic exergy of hot stream. The trend of variation of hot end exergy agrees well with that of Dincer et al. [10]. Figure 13 shows the comparison of the results of Dincer et al. [10] and the current study for total lost exergy for various values of cold mass ratio. In the present work, higher exergy loss is detected at higher values of cold mass

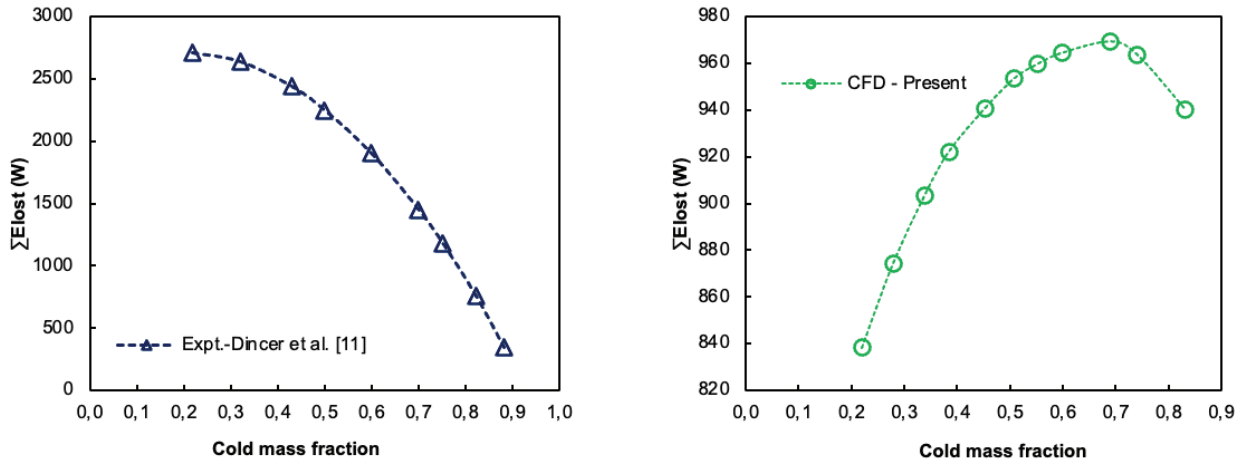

(a) (b)

Figure 13. (a) Total lost exergy at different cold mass ratios in Dincer et al. [10] (made by author).

ratio contrary to the observations of Dincer et al. [10]. The magnitude of total lost exergy observed in the present work is comparatively lesser. Also, total lost exergy as observed from Fig. 10 (b) increases up to certain cold mass ratio and then decreases. Hence, it was felt necessary to re-examine this behaviour for different inlet pressures and hence total lost exergy was calculated for entry pressure values of 200 kPa, 300 kPa, 400 kPa, 500 kPa and 600 kPa. These are presented in Figure 14 to Figure 19. These values are also compared with each other as shown in Figure 20. These figures indicate a similar trend with regard to lost exergy for different cold mass ratios and thus the trend is confirmed. This can be attributed to dissimilar geometrical parameters of VT and entry pressures used in the present work. With a rise in entry pressure, the magnitude of total lost exergy also increases.

As observed from Figure 20, the magnitude of lost exergy is higher with rise in entry pressure for all values of cold mass ratio. At a particular entry pressure, lost exergy magnitude first improves up to certain cold mass ratio in the range of 0.5 to 0.7 and thereafter again reduces for succeeding cold mass ratios. The maximum magnitude of lose exergy was observed to be 424.55 W at 200 kPa, 708.04 W at 300 kPa, 950.47 W at 400 kPa, 1184. 38 at 500 kPa and 1473.91 W at 600 kPa inlet pressure.

Figure 21 depicts the deviation of exergy efficiency of hot stream and cold for various cold mass ratio values. With an increase in cold mass ratio, the hot end exergy efficiency

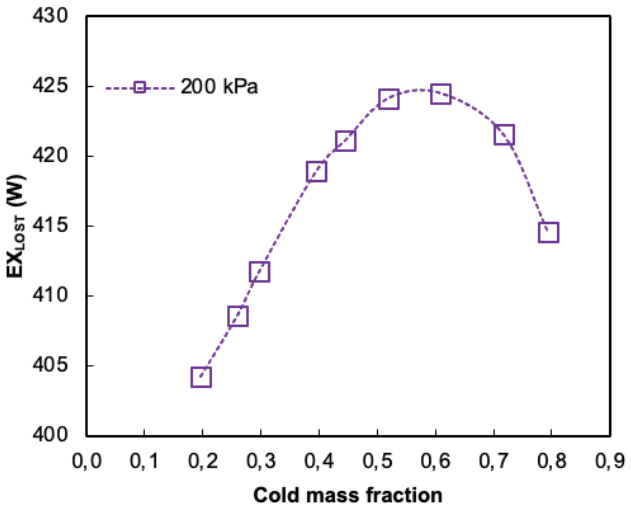

Figure 14. Exergy loss at 200 kPa for various cold mass ratios.

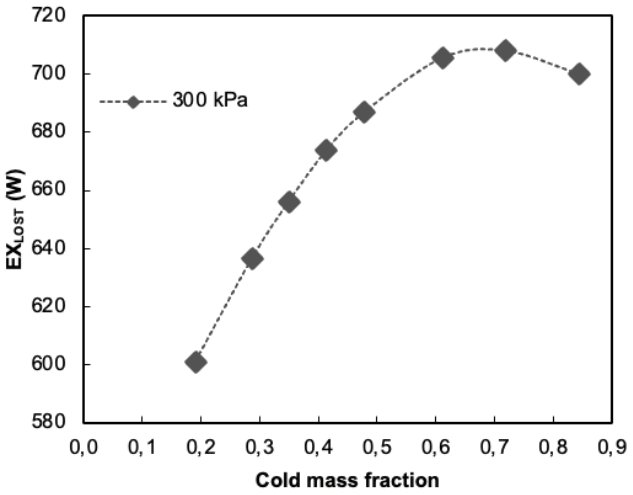

Figure 15. Exergy loss at 300 kPa and various cold mass ratios.

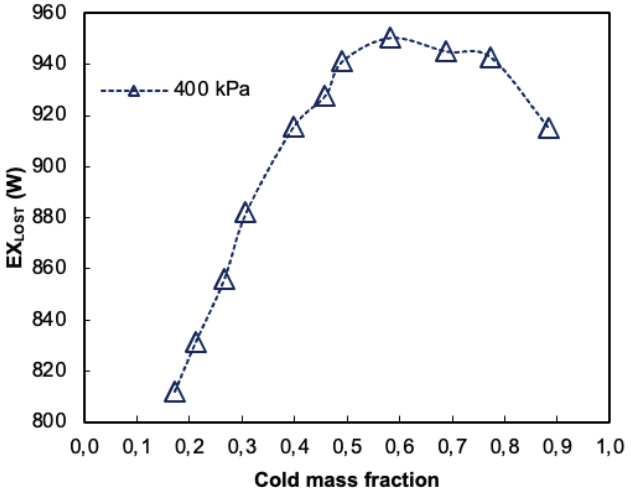

Figure 16. Exergy loss at 400 kPa and various cold mass ratios.

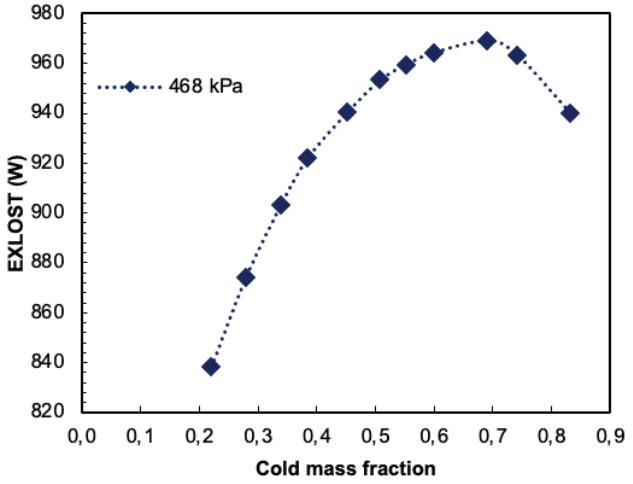

Figure 17. Exergy loss at 468 kPa and various cold mass ratios.

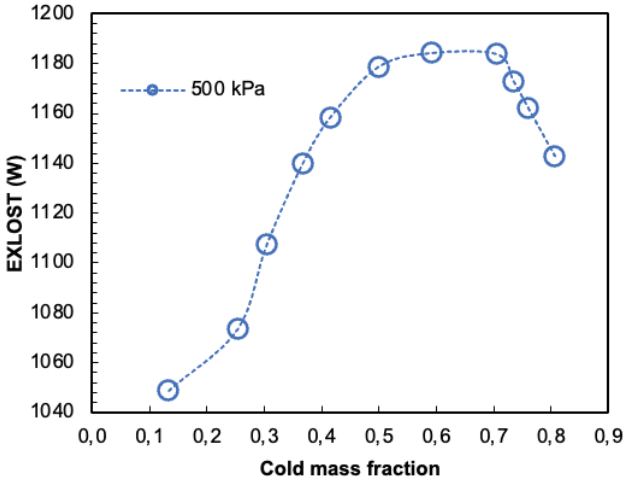

Figure 18. Exergy loss at 500 kPa and various cold mass ratios.

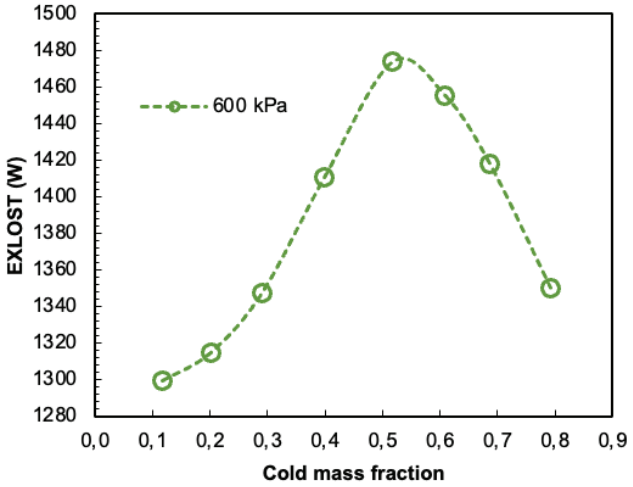

Figure 19. Exergy loss at 600 kPa and various cold mass ratios.

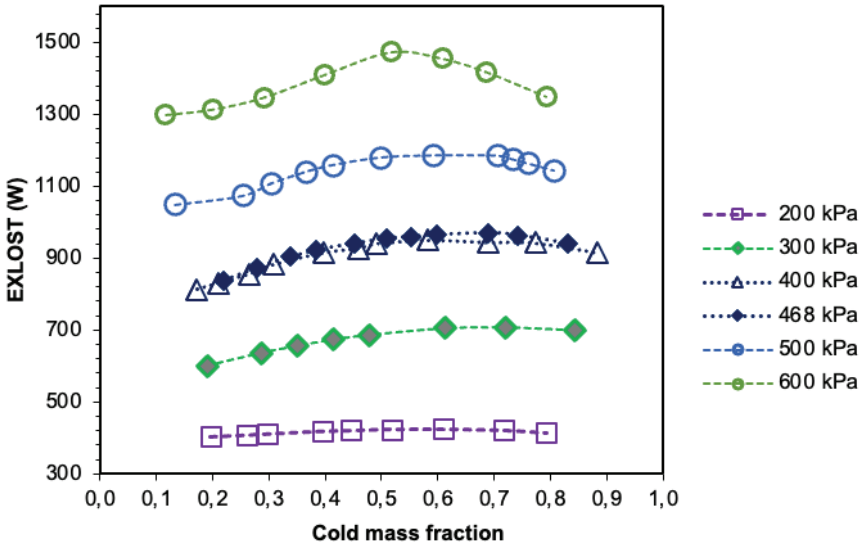

Figure 20. Comparison of the magnitude of lost exergy for different entry pressures and cold mass ratios.

reduces due to reduced mass flow rate through hot exit. The qualitative trend of exergy efficiency observed in the present work agrees well with that of Dincer et al. [10]. With higher in cold mass ratio, the cold exit exergy efficiency increases due to increased mass flow rate through the cold exit. The qualitative trend of exergy efficiency observed in the present work agrees well with that of Dincer et al. [10].

Figure 22 shows the variation of cold outlet exergy as well as cold end exergy efficiency for several values of cold mass ratio and entry pressure. The exergy magnitude for the lower cold mass ratio is similar for all inlet pressures. The quantum of exergy starts differing for various pressures once the cold mass ratio is more than 0.4. With a rise in entry pressure, the magnitude of cold outlet exergy increases for all cold mass ratio values. The maximum cold end exergy magnitude is observed to be 84.02 W at 200 kPa, 193.04 W at 300 kPa, 353.88 W at 400 kPa, 437.06 W at 500 kPa, and 604.09 W at 600 kPa inlet pressure. Figure 21 and Figure 22 signify that higher cold mass ratio values are useful when VT is being used for cooling applications. The trend of cold-end exergy magnitude and cold-end exergy efficiency are similar to each other. With increase in cold mass ratio, higher mass of air exits through the cold outlet, which results in higher velocity. This increases the magnitude of kinetic and physical exergy at cold outlet. The maximum exergy efficiency is observed to be 15.58% at 200 kPa,

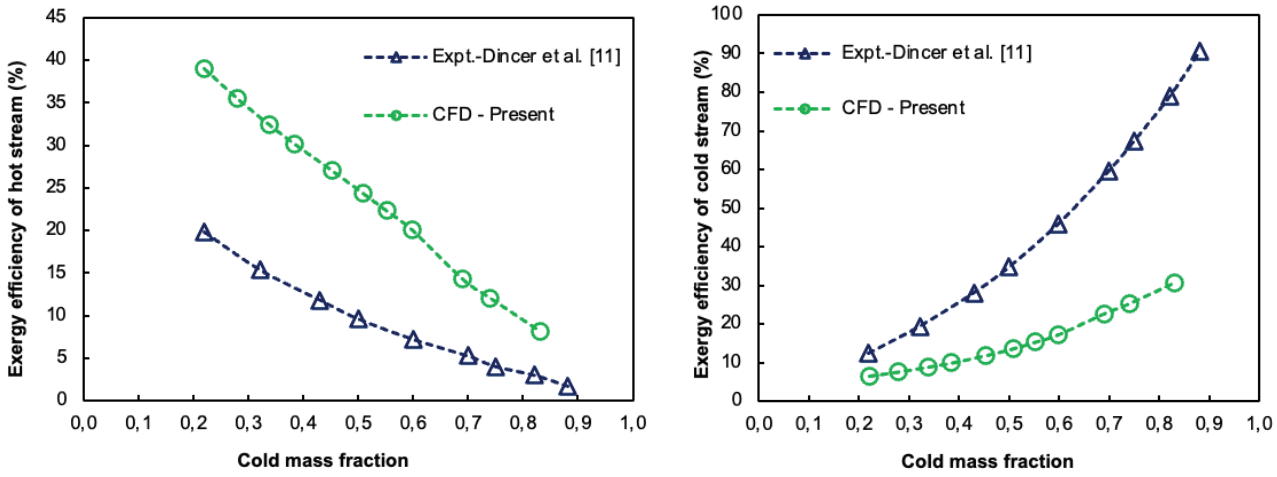

(a) (b)

Figure 21. (a) Exergy efficiency of hot exit for various cold mass ratios (b) Exergy efficiency of cold exit for various cold mass ratios.

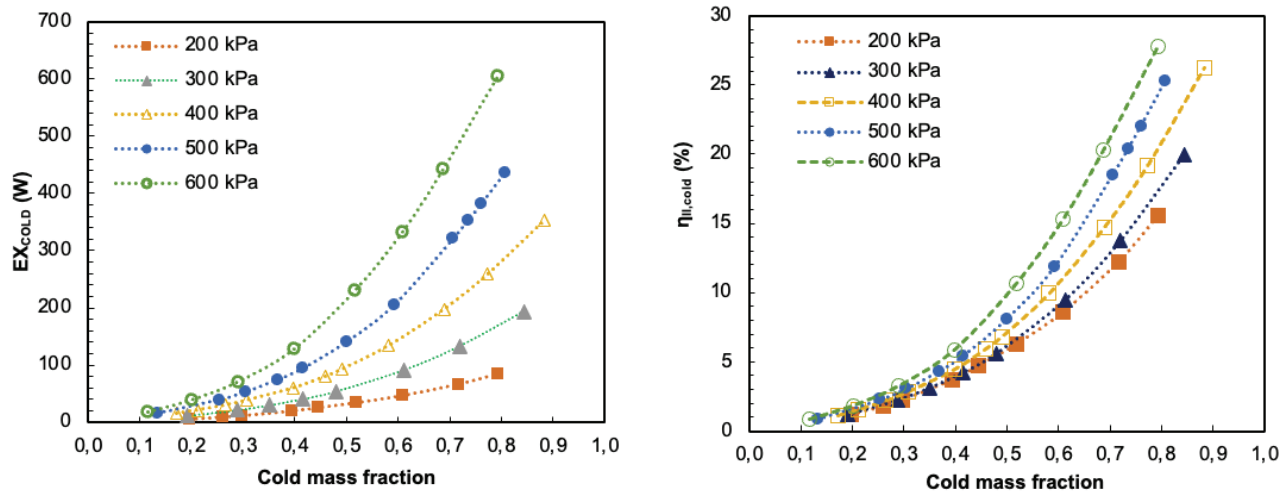

(a) (b)

Figure 22. (a) Cold exit exergy for various cold mass ratios and inlet pressures (b) Cold end exergy efficiency for different cold mass ratios and inlet pressures.

19.98% at 300 kPa, 26.21% at 400 kPa, 25.23% at 500 kPa and 27.77% at 600 kPa inlet pressure. The difference of rise in efficiency is higher at lower pressure values compared to that of higher-pressure values.

Figure 23 shows the variation of hot outlet exergy for various values of cold mass ratio and inlet pressure values. With the rise in cold mass ratio i.e., a decline in hot side mass flow rate, exergy magnitude at the hot side reduces. This observation is consistent with that of Bej and Sinhamahapatra [14]. With an increase in cold mass ratio, the hot end exergy efficiency reduces due to reduced mass flow rate through hot exit. Reduction in the mass flow rate at hot end also lowers the magnitude of kinetic and physical exergy, thereby reducing the efficiency. As the cold fraction reduces, the mass flow rate of hot gas increases, thereby stimulating the energy separation and higher hot-end exergy due to vigorous momentum transfer.

At any cold mass ratio, the magnitude of hot end exergy increases with inlet pressure. The lowest magnitude of exergy efficiency is detected for lower entry pressure value of 200 kPa. After this inlet pressure, exergy efficiency increases with rise in inlet pressure. Interestingly, exergy efficiency shows almost similar values for higher values of inlet pressures for the complete series of cold mass ratio.

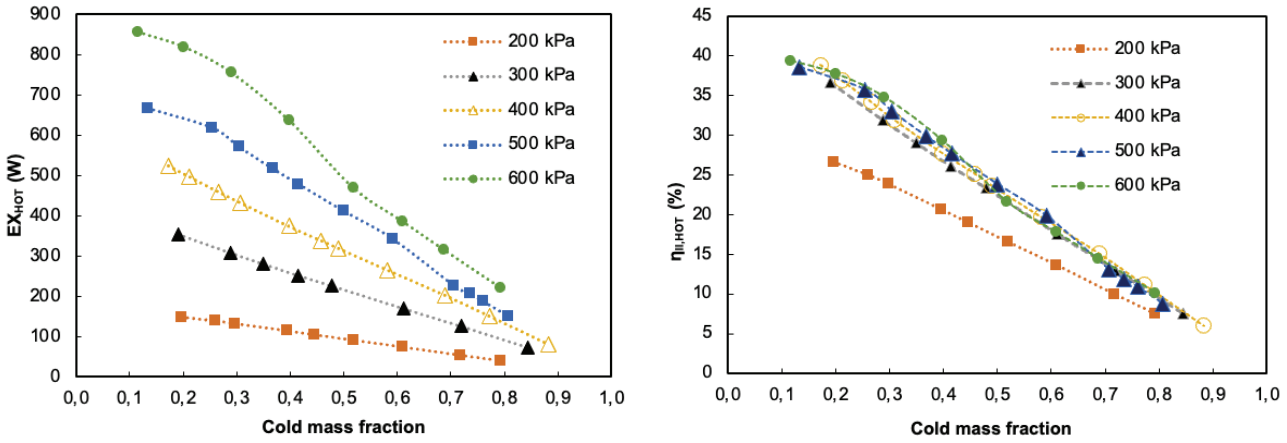

(a) (b)

Figure 23. (a) Hot end exergy for various cold mass ratios and entry pressures (b) Hot end exergy efficiency for various cold mass ratios and entry pressures.

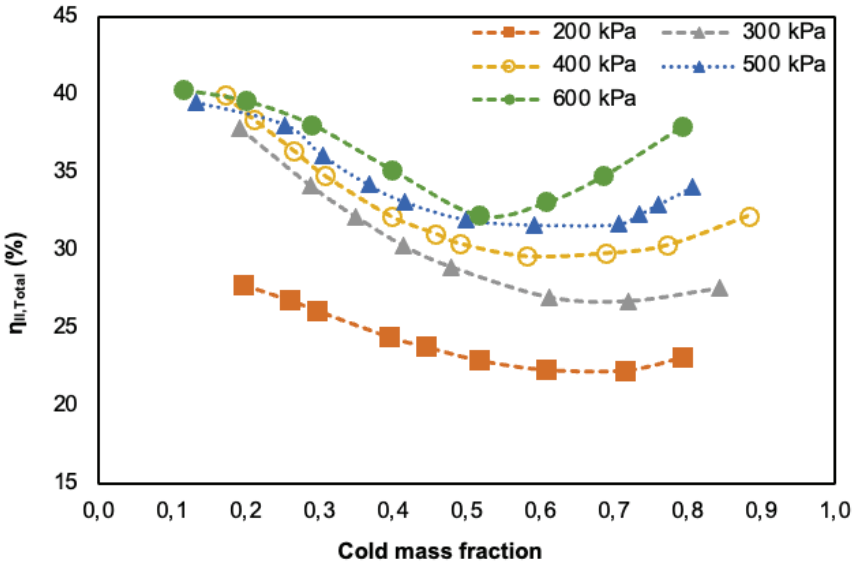

Figure 24. Total exergy efficiency for different inlet pressures and cold mass ratios.

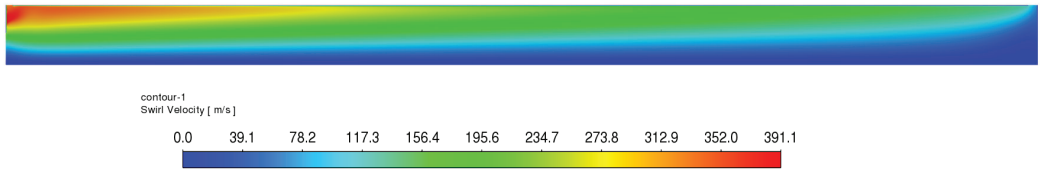

Figure 25. Contours of swirl velocity in VT at 600 kPa inlet pressure.

Thus, cold-end exergy efficiency is more influenced by entry pressure than hot-end exergy efficiency. The maximum hot end exergy magnitude is observed to be 148.85 W at 200 kPa, 353.80 W at 300 kPa, 525.25 W at 400 kPa, 667.97 W at 500 kPa and 856.60 W at 600 kPa inlet pressure. The maximum hot-end exergy efficiency is 26.59% at 200 kPa, 31.89% at 300 kPa, 38.83 % at 400 kPa, 38.55% at 500 kPa and 39.39% at 600 kPa.

Figure 24 shows the variation of total exergy efficiency of VT for different entry pressures and cold mass ratio

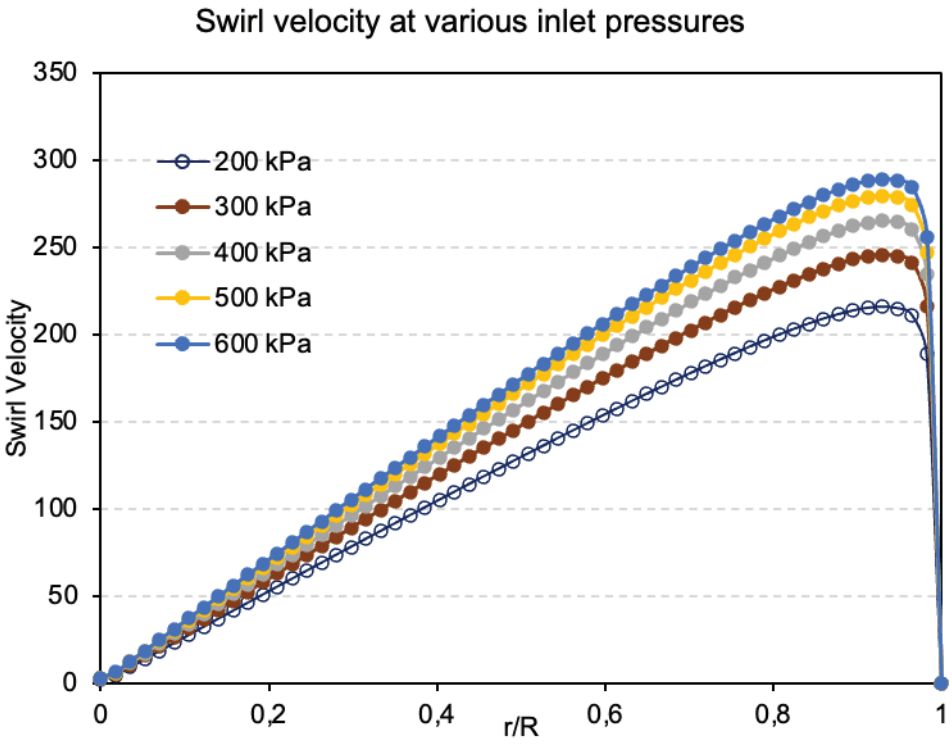

Figure 26. Swirl velocity in radial direction for various inlet pressures.

values. The total exergy efficiency firstly reduces when the cold mass ratio is increased and thereafter it increases. This trend is observed for all the inlet pressures. Maximum total exergy efficiency is observed to be 27.76% at 200 kPa, 37.78% at 300 kPa, 39.94% for 400 kPa, 39.45% at 500 kPa, and 40.23% for 600 kPa inlet pressure at lower values of cold mass ratio. Instead, at higher cold mass ratio, maximum total exergy efficiency is observed to be 23.08% at 200 kPa, 27.53% at 300 kPa, 32.19% for 400 kPa, 34.01% at 500 kPa and 37.90% for 600 kPa entry pressure. For all the entry pressures, minimum total exergy is gained in the cold mass ratio range of 0.4 to 0.6.

To explore the flow physics further, variation of swirl velocity inside VT has been demonstrated in Figure 25. It indicates that at the core of VT, magnitude of swirl velocity is minimal. Highest swirl velocity is observed right at the inlet of VT wherein expansion of pressure raised air pressurised air takes place during entry. To check this effect for various inlet pressures, swirl velocity has been plotted as observed in Figure 26. It is noteworthy that this graph has been plotted through 870 data points. It clearly indicates that swell velocity in the axial zone is minimal and increases progressively towards the outer radius of VT and right near the wall, the magnitude of swirl velocity suddenly diminishes due to contact of fluid with wall of VT. When this is compared with inlet exergy, it is observed that both inlet egg surgery and swirl velocity exergy and swell velocity increase with inlet pressure since swirl velocity constitutes the largest component of inlet total velocity of pressurised fluid.

CONCLUSION

Computational analysis of vortex tube was performed to understand the result of change in entry pressure and cold mass ratio on exergy parameters. The following are conclusions drawn from present study:

1. The computational model is able to replicate the compressible, turbulent, swirling flow inside the vortex tube with substantial accuracy. Such a model can be useful as complementary for experimental investigation.
2. Novelty of present work is that it explores interactive effect of various values of cold mass fraction and inlet pressure on exergy parameters of VT, unlike previous works wherein cold mass fraction has been kept constant.
3. Exergy parameters such as cold and hot end outlet exergy, and exergy efficiency are significantly affected by cold mass ratio. Hence, unlike previous works, investigations should be carried out for various cold mass ratios as well.
4. Cold exit exergy efficiency increases and hot end exergy efficiency declines with an increase in cold mass ratio. Cold-end exergy efficiency is more influenced by entry pressure than hot-end exergy efficiency. The total exergy efficiency shows a minimum value for cold mass ratios in the range of 0.4 to 0.6.
5. The observations reported in the current numerical study are consistent with previously published numerical and experimental works. The results shall be useful while making operational choices during the practical application of vortex tube.

6. Limitation of current methodology is that it is only as good as the observations recorded, either during experimentation or computational analysis. If the researchers are focusing more towards enhancing the accuracy of their measurements / computational results, then enhanced understanding can be still developed. This is a potential area for improvement.
7. Further, research work can be undertaken to understand the effect of various geometric and operational parameters on exergy efficiency such as length to diameter ratio, cold end diameter, working fluids and inlet pressures.

NOMENCLATURE

Cp	specific heat at constant pressure, kJ kg^{-1} K^{-1}
D	VT diameter, mm
E	exergy level of the stream, W
h	enthalpy of fluid, kJ kg^{-1}
k	thermal conductivity of fluid, Wm^{-1} K^{-1}
m	mass flow rate of fluid, kg s^{-1}
P	various pressure values, kPa
T	Temperature, K

Greek symbols

μ_c	dimensionless cold mass ratio
ρ	air density, kg m^{-3}
η	exergy efficiency

Subscripts

c	quantity at the cold side
h	quantity at the hot side
i	quantity at the inlet
max	maximum value

UPDATED NOMENCLATURE

Cp	specific heat at constant pressure, kJ kg^{-1} K^{-1}
D	VT diameter, mm
E	Energy level of the stream, W
$\dot{E}$	Exergy level of the stream, W
h	enthalpy of fluid, kJ kg^{-1}
k	thermal conductivity of fluid, Wm^{-1} K^{-1}
m	mass flow rate of fluid, kg s^{-1}
P	various pressure values, kPa
P_0	reference environmental pressure, kPa
T	Temperature, K
ΔT	Temperature separation magnitude, K
T_0	initial reference environment temperature 293.15 K,
R	specific gas constant, kJ kg^{-1} K^{-1}
v	velocity of the fluid stream, m s^{-1}

Greek symbols

μ_c	dimensionless cold mass ratio
ρ	air density, kg m^{-3}
η	exergy efficiency

Subscripts

c	quantity at the cold side
h	quantity at the hot side
i	quantity at the inlet
max	maximum value

ACKNOWLEDGMENT

The author is also grateful to Hon. Management of Shri Vile Parle Kelavani Mandal's Institute of Technology, Dhule & Principal Dr. Nilesh Salunke for providing computational support during this research. Special thanks are also due to Dr. Bhushan Behede, Assistant Professor, Dept. of Mechanical Engineering, SVKM's Institute of Technology, Dhule for his help and support with operating the Mendeley software.

AUTHORSHIP CONTRIBUTIONS

Authors equally contributed to this work.

DATA AVAILABILITY STATEMENT

The authors confirm that the data that supports the findings of this study are available within the article. Raw data that support the finding of this study are available from the corresponding author, upon reasonable request.

CONFLICT OF INTEREST

The author declared no potential conflicts of interest with respect to the research, authorship, and/or publication of this article.

ETHICS

There are no ethical issues with the publication of this manuscript.

STATEMENT ON THE USE OF ARTIFICIAL INTELLIGENCE

Artificial intelligence was not used in the preparation of the article.

REFERENCES

[1] Joseph RG. Method and apparatus for obtaining from alpha fluid under pressure two currents of fluids at different temperatures. US patent 1,952,281. 1934.

[2] Hilsch R. The use of the expansion of gases in a centrifugal field as cooling process. Rev Sci Instrum 1947;18:108−13. [CrossRef]

[3] Wu YT, Ding Y, Ji YB, Ma CF, Ge MC. Modification and experimental research on vortex tube. Int J Refrig 2007;30:1042−9. [CrossRef]

[4] Kırmacı V. Exergy analysis and performance of a counter flow Ranque–Hilsch vortex tube having various nozzle numbers at different inlet pressures of oxygen and air. Int J Refrig 2009;32:1626–33. [CrossRef]
[5] Thakare HR, Parekh AD. Experimental investigation of Ranque—Hilsch vortex tube and techno–economical evaluation of its industrial utility. Appl Therm Eng 2020;169:114934. [CrossRef]
[6] Saidi MH, Yazdi MA. Exergy model of a vortex tube system with experimental results. Energy 1999;24:625–32. [CrossRef]
[7] Aljuwayhel NF, Nellis GF, Klein SA. Parametric and internal study of the vortex tube using a CFD model. Int J Refrig 2005;28:442–50. [CrossRef]
[8] Tarasova L, Troshkin O, Shilin M, Tsvetkov A. The scope for using a vortex tube as a dust trap. Chem Pet Eng 2009;45:443–5. [CrossRef]
[9] Kırmacı V, Uluer O, Dincer K. An experimental investigation of performance and exergy analysis of a counterflow vortex tube having various nozzle numbers at different inlet pressures of air, oxygen, nitrogen, and argon. J Heat Transf 2010;132:121701. [CrossRef]
[10] Dincer K, Yilmaz Y, Berber A, Baskaya S. Experimental investigation of performance of hot cascade type Ranque–Hilsch vortex tube and exergy analysis. Int J Refrig 2011;34:1117–24. [CrossRef]
[11] Dutta T, Sinhamahapatra KP, Bandyopadhyay SS. Numerical investigation of gas species and energy separation in the Ranque–Hilsch vortex tube using real gas model. Int J Refrig 2011;34:2118–28. [CrossRef]
[12] Ouadha A, Baghdad M, Addad Y. Effects of variable thermophysical properties on flow and energy separation in a vortex tube. Int J Refrig 2013;36:2426–37. [CrossRef]
[13] Khazaei H, Teymourtash AR, Malek-Jafarian M. Effects of gas properties and geometrical parameters on performance of a vortex tube. Sci Iran 2012;19:454–62. [CrossRef]
[14] Bej N, Sinhamahapatra KP. Exergy analysis of a hot cascade type Ranque-Hilsch vortex tube using turbulence model. Int J Refrig 2014;45:13–24. [CrossRef]
[15] Manimaran R. Computational analysis of flow features and energy separation in a counter-flow vortex tube based on number of inlets. Energy 2017;123:564–78. [CrossRef]
[16] Moraveji A, Toghraie D. Computational fluid dynamics simulation of heat transfer and fluid flow characteristics in a vortex tube by considering the various parameters. Int J Heat Mass Transf 2017;113:432–43. [CrossRef]
[17] Devade KD, Pise AT. Exergy analysis of a counter flow Ranque–Hilsch vortex tube for different cold orifice diameters, L/D ratios and exit valve angles. Heat Mass Transf 2017;53:2017–29. [CrossRef]
[18] Kirmaci V, Kaya H, Cebeci I. An experimental and exergy analysis of a thermal performance of a counter flow Ranque–Hilsch vortex tube with different nozzle materials. Int J Refrig 2018;85:240–54. [CrossRef]
[19] Jain G, Arora A, Gupta SN. Exergy analysis of the transcritical N2O refrigeration cycle with a vortex tube. Int J Green Energy 2018;15:507–16. [CrossRef]
[20] Kaya H, Uluer O, Kocaoğlu E, Kirmaci V. Experimental analysis of cooling and heating performance of serial and parallel connected counter-flow Ranquee–Hilsch vortex tube systems using carbon dioxide as a working fluid. Int J Refrig 2019;106:297–307. [CrossRef]
[21] Aghagoli A, Sorin M. Thermodynamic performance of a CO2 vortex tube based on 3D CFD flow analysis. Int J Refrig 2019;108:124–37. [CrossRef]
[22] Lagrandeur J, Croquer S, Poncet S, Sorin M. Exergy analysis of the flow process and exergetic optimization of counterflow vortex tubes working with air. Int J Heat Mass Transf 2020;152:119527. [CrossRef]
[23] Wang Z, Suen KO. Numerical comparisons of the thermal behaviour of air and refrigerants in the vortex tube. Appl Therm Eng 2020;164:114515. [CrossRef]
[24] He P, Liang Y, Hu Y, Zhang C, Zhang D, Ai X, et al. Effect of physical properties of a gas on the refrigeration temperature drop of vortex tubes used in oil and gas fields. ACS Omega 2021;6:31738–50. [CrossRef]
[25] Jain G, Arora A, Gupta SN. Exergy analysis of a vortex tube expansion two-stage transcritical N2O refrigeration cycle. Int J Ambient Energy 2022;43:4757–66. [CrossRef]
[26] Liang F, Tang G, Xu C, Wang C, Wang Z, Wang J, et al. Experimental investigation on improving the energy separation efficiency of vortex tube by optimizing the structure of vortex generator. Appl Therm Eng 2021;195:117222. [CrossRef]
[27] Shahsavar A, Jahangiri A, Ahmadi G. Energy and exergy analysis and multi-objective optimization of using combined vortex tube-photovoltaic/thermal system in city gate stations. Renew Energy 2022;196:1017–28. [CrossRef]
[28] Jahangiri A, Ameri M, Ahmadi G, Shahsavar A. Performance analysis of vortex tube-thermoelectric system in gas stations. Sustain Energy Technol Assess 2022;53:102522. [CrossRef]
[29] Yadav GMP, Reddy PM, Gowd BUM. Effect of end control plugs on the performance of vortex tube with dual forced vortex flow. J Therm Eng 2016;2:871–81. [CrossRef]
[30] Devade K. Parametric analysis of thermal performance of Ranque-Hilsch vortex tube. J Therm Eng 2018;4:2333–54. [CrossRef]
[31] Noor D, Mırmanto H, Sarsetiyanto J, Soedjono D. Flow behavior and thermal separation mechanism on vortex tube. J Therm Eng 2021;7:1090–9. [CrossRef]

[32] Bagre N, Parekh AD, Patel VK. A CFD investigation of flow separation in an elliptical and circular Ranque-Hilsch vortex tube. J Therm Eng 2023;9:414–28. [CrossRef]
[33] Ahlborn B, Groves S. Secondary flow in a vortex tube. Fluid Dyn Res 1997;21:73–86. [CrossRef]
[34] Skye HM, Nellis GF, Klein SA. Comparison of CFD analysis to empirical data in a commercial vortex tube. Int J Refrig 2006;29:71–80. [CrossRef]
[35] Farouk T, Farouk B. Large eddy simulations of the flow field and temperature separation in the Ranque–Hilsch vortex tube. Int J Heat Mass Transf 2007;50:4724–35. [CrossRef]
[36] Shamsoddini R, Nezhad AH. Numerical analysis of the effects of nozzles number on the flow and power of cooling of a vortex tube. Int J Refrig 2010;33:774–82. [CrossRef]
[37] Dutta T, Sinhamahapatra KP, Bandyopdhyay SS. Comparison of different turbulence models in predicting the temperature separation in a Ranque–Hilsch vortex tube. Int J Refrig 2010;33:783–92. [CrossRef]
[38] ANSYS Inc. FLUENT 6.3 validation guide. 2006.
[39] Pourmahmoud N, Akhesmeh S. Numerical investigation of the thermal separation in a vortex tube. World Acad Sci Eng Technol 2008;19:399–405.
[40] Stephan K, Lin S, Durst M, Huang F, Seher D. A similarity relation for energy separation in a vortex tube. Int J Heat Mass Transf 1984;27:911–20. [CrossRef]